

# FLOW AND THERMAL PERFORMANCE OF AN AIRFOIL-ENDWALL FILLET FOR A GAS TURBINE NOZZLE GUIDE VANE

Stephen Lynch

Mechanical Engineering, Virginia Tech

Advisor: Karen A. Thole

Mechanical & Nuclear Engineering, The Pennsylvania State University

## Abstract

Gas turbine engines are used in a variety of power generation applications, including providing thrust for the F-35 Lightning II Joint Strike Fighter, turning electrical generators in combined-cycle power plants, and powering the M1 Abrams Main Battle Tank. In the high-temperature region of the turbine section, a complex vortical (swirling) flow present near the junction of a turbine airfoil and its casing (endwall) tends to decrease aerodynamic efficiency and increase metal temperatures. Past research indicates a large fillet at the airfoil-endwall junction can help to mitigate the effects of the endwall vortical flow. Also, leakage flow through inherent gaps between individually manufactured turbine components can interfere with the endwall vortical flow. This research discusses the effect of two types of leading edge airfoil-endwall fillets, with and without leakage flow from a two-dimensional slot simulating the combustor-turbine gap. Measurements of aerodynamic loss were obtained at the exit of a nozzle guide vane cascade at matched engine Reynolds number conditions. Results showed that without leakage flow, the fillets slightly reduced aerodynamic loss. The addition of leakage flow from the combustor-turbine interface gap increased losses by 14% for the linear-profile fillet but did not increase losses for the elliptical-profile fillet, indicating that a thorough understanding of the inlet flow conditions is critical in the design of a fillet.

## Introduction

Gas turbines are a popular choice for motive power for aircraft because of their high thrust-to-frontal drag area and power-to-weight ratios. They also provide shaft power for electricity generation in power plants, where their relatively rapid response to varying electric load demands and minimal installation requirements is an advantage. Significant increases in gas turbine efficiency and power output have been achieved by increasing the temperature of the combustion products entering the turbine section, to the point that current turbines operate with combustion gas temperatures on the order of 300°C higher than the melting point of the metal components. Innovative cooling schemes, such as bleeding air from the compressor section through the

core of a part and then ejecting it through holes in its surface, are required to maintain part integrity.

The endwall region of a turbine vane or blade is particularly important to cool because of the presence of a complex flow that develops at the airfoil-endwall junction. Flow models, such as the one presented by Langston<sup>1</sup> and depicted in Figure 1, describe an approaching boundary layer on the endwall that rolls up into a horseshoe vortex at the leading edge of the vane. The horseshoe vortex splits into suction and pressure side legs, and the pressure side leg develops into a larger passage vortex. These vortical structures, generally termed secondary flows, can be a large source of aerodynamic loss. Secondary flows also sweep coolant from the endwall and increase endwall heat transfer.

Several methods to control or eliminate secondary flows have been tested, including blowing, three-dimensional endwall contouring, and modification of the leading-edge endwall-airfoil junction. Adding a fillet to the endwall-airfoil junction has been shown to be particularly successful in increasing aerodynamic efficiency and reducing endwall heat transfer by inhibiting the formation of the horseshoe vortex.

In an engine, gaps are present between individually manufactured components, and cool air from the compressor is allowed to leak through the gaps. This prevents hot gas ingestion, and can provide some

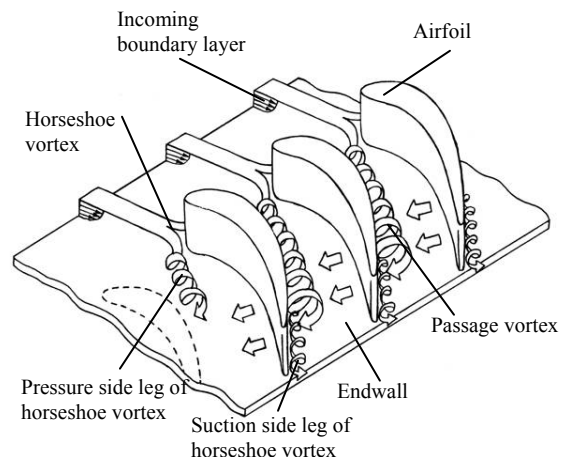


Figure 1. Secondary flow model presented by Langston<sup>1</sup>.

cooling to the part surface. A particular gap of interest is between the combustor and the turbine. Leakage flow from this gap interacts with the secondary flow, and at high flow rates the coolant may interfere with secondary flow development.

This paper presents experimental measurements of the combined effect of combustor-turbine interface leakage and a large leading-edge fillet on the overall aerodynamic losses. The results are compared with previously described measurements of adiabatic film-cooling effectiveness. The objective of this study is to explore the interaction of the fillet with combustor-turbine gap leakage flow.

### **Relevant Past Studies**

Active and passive methods have been proposed to control or eliminate the development of the horseshoe and passage vortices, including blowing, three-dimensional endwall contouring, and leading edge endwall-airfoil geometries. However, these methods are rarely considered simultaneously in research to date, and in the case of an engine with a leakage interface, the interaction of leakage flow with endwall contouring or a fillet can result in unexpected behavior.

Past research has shown that for a canonical turbulent inlet boundary layer, modifications to the leading edge of a gas turbine vane can reduce or eliminate some of the features of the secondary flow. Sauer et al.<sup>2</sup> presented experimental measurements showing a remarkable 47% reduction in net aerodynamic losses for an asymmetric leading edge bulb which was designed to intensify the suction side leg of the horseshoe vortex, and thus cancel the effect of the counter-rotating passage vortex. Zess and Thole<sup>3</sup> computationally studied several fillet designs, and experimentally tested an asymmetric linear-profile design. Measurements indicated elimination of the horseshoe vortex and an order of magnitude reduction in turbulent kinetic energy levels associated with vortex development. Becz et al.<sup>4</sup> tested a bulb based on the design of Sauer et al.<sup>2</sup>, as well as an asymmetric elliptical fillet, and found that only the fillet reduced overall mass-averaged total pressure loss.

Other studies have focused on the thermal aspects of an endwall-airfoil juncture modification. Lethander et al.<sup>5</sup> coupled an optimization routine with a commercial computational flow solver to design a relatively large fillet, with dimensions at the limits of their design space, that reduced adiabatic wall temperatures in the presence of simulated combustor cooling flow. Streamlines indicated elimination of the horseshoe vortex for the large fillet, although the fillet exhibited a slight increase in mass-averaged total pressure loss relative to an unfilleted endwall. Han and Goldstein<sup>6</sup> used naphthalene sublimation to infer heat transfer distributions on the endwall through the heat

and mass transfer analogy. Their linear asymmetric fillet, based on the design by Zess and Thole<sup>3</sup>, reduced the horseshoe vortex but resulted in increased heat transfer at the endwall-airfoil junction downstream of the fillet due to intensified corner vortices. The measurements and computations of Mahmood et al.<sup>7</sup> and Saha et al.<sup>8</sup> for linear and circular-profile fillet geometries indicated that fillets reduced the leading edge vortex size and slightly lowered endwall heat transfer coefficients relative to an unfilleted airfoil, with a concave circular geometry showing slightly more reduction in heat transfer than other geometries. However, total pressure losses were not reduced with any of the fillets.

Several studies have considered the thermal and aerodynamic effect of leakage flow introduced through the combustor-turbine interface gap upstream of the nozzle guide vane. Blair's<sup>9</sup> measurements of endwall adiabatic cooling effectiveness from leakage flow through a two-dimensional flush slot upstream of the vane showed coolant accumulating at the suction side corner of the vane-endwall junction, which would be attributed to the sweeping effect of the passage vortex. This effect has been corroborated by the many subsequent studies of leakage flow upstream of an airfoil. However, coolant can influence secondary flow physics under the right conditions. A computational study by Knost and Thole<sup>10</sup> showed that near-wall streamlines became increasingly directed toward the pressure side of the vane as the flow rate through their two-dimensional flush slot was increased. From measurements in a transonic cascade, Kost and Nicklas<sup>11</sup> found that leakage flow from their flush slot, positioned  $0.2C_{ax}$  upstream of the vane, significantly strengthened the horseshoe vortex. This was attributed to the slot injecting at the separation location on the endwall. Pitchwise-averaged losses showed that slot injection shifted the loss peak (attributable to the passage vortex) slightly away from the endwall, as well as increasing area-averaged losses relative to no injection. In Kost and Mullaert's<sup>12</sup> subsequent study, the slot was positioned farther upstream (at  $0.3C_{ax}$  upstream of the vane), which helped coolant stay close to the endwall and spread more uniformly. In contrast to the results of Kost and Nicklas<sup>11</sup>, the aerodynamic measurements of Burd and Simon<sup>13</sup> for leakage flow from a flush slot on an axisymmetric contoured endwall revealed that the leakage flow did not impact the total pressure loss in the cascade. However, axisymmetric contouring has been shown to suppress secondary flow and thus would be expected to minimize its interaction with leakage coolant. Burd et al.<sup>14</sup> concluded from thermal measurements in the same cascade that coolant at low flow rates was strongly influenced by secondary flow, but coolant at a high flow rate of 3.2% of the cascade inlet flow provided optimum coverage because

its high momentum enabled it to avoid being entrained by secondary flow vortices.

This study is the first to present the combined effect of combustor-turbine interface leakage flow and a large fillet at the endwall-airfoil junction. The interaction of the two will provide additional insight into the development of the complex endwall secondary flow, and its effect on turbine aerodynamics and heat transfer.

### **Experimental Facility and Methodology**

Velocity, flow angles, and total pressure were measured at the exit of a nozzle guide vane test section in a closed-loop low-speed wind tunnel. The tunnel, illustrated in Figure 2, had an axial fan that drove the flow through the closed loop. A porous plate diverted some of the flow into bypass channels, where it could be cooled and pumped into a supply plenum for film coolant injection studies. The core channel flow that was not diverted could be heated with a 55kW heater bank, to simulate hot mainstream flow. For the aerodynamic studies presented here, no flow heating or cooling was utilized.

The nozzle guide vane test section is depicted in Figure 3. The test section contained two flow passages, defined by two full nozzle guide vanes and a third partial vane connected to a flexible wall. The flexible wall was adjusted to maintain the desired pressure distribution around the center vane. The vanes, based on the midspan geometry of a commercial aircraft engine nozzle guide vane, were scaled by a factor of nine from the engine and were constructed of low thermal conductivity foam. The nozzle guide vane parameters are given in Table 1.

A turbulent boundary layer was measured at  $0.63C$  upstream of the vane on the bottom endwall. The boundary layer had a thickness of  $\delta/S=0.18$ , a momentum thickness of  $\theta/S=0.020$ , a shape factor  $H=1.26$ , and a momentum Reynolds number  $Re_\theta=4138$ . The tunnel nominal turbulence intensity and length scale, measured at the cascade inlet, were 0.7% and 4 cm (0.07C), respectively.

### **Combustor-Turbine Interface Leakage Geometry**

The leakage interface between a combustor and a turbine was modeled by a two-dimensional slot placed on the bottom endwall of the nozzle guide vane test section, as seen in Figure 3. The interface will be referred to as an upstream slot in this paper. The leakage interface was based on the geometry of Cardwell et al.<sup>15</sup>, who consulted industrial contacts to design a representative leakage interface. The upstream slot metering width, scaled to nine times that of the engine, was 1.43 cm (0.024C). Note that the slot location, at  $0.77C_{ax}$  upstream of the vane, has been moved significantly upstream from the location studied

by Cardwell et al.<sup>15</sup>, who positioned their slot at  $0.3C_{ax}$  upstream. The increased upstream distance of the slot was necessary to accommodate the airfoil-endwall junction geometries studied here.

The leakage flow was supplied from a plenum located underneath the bottom endwall. The plenum supply was extracted from the top bypass channel of the wind tunnel by a blower (see Figure 2). To determine the average mass flow through the slot, the inviscid blowing ratio of the slot was multiplied by an assumed discharge coefficient of 0.6 (the commonly-accepted value for a sharp-edged orifice<sup>16</sup>). Mass flow through the slot is reported as a percentage of the mass flow entering a single vane passage. Only a single mass flow rate has been studied to-date and is presented here. The leakage flow rate of 1.0% of the cascade flow was assumed to be a representative value from engine conditions. The coolant-to-mainstream density ratio was 1.0 for all studies. For the studies without leakage flow, the slot geometry was not present.

### **Airfoil-Endwall Junction Geometries**

Two large leading-edge fillet designs were chosen for comparison with a standard  $90^\circ$  endwall-airfoil junction. The two geometries, illustrated in Figure 4, were designed with a linear endwall-to-airfoil profile (referred to as a linear fillet), and an elliptical endwall-to-airfoil profile (referred to as an elliptical fillet), respectively. The geometry of the fillets followed the methodology of the computational optimization study by Lethander et al.<sup>5</sup> The extent of the fillet outward from the vane, as well as the height of the fillet from

**Table 1. Vane Geometry and Flow Conditions**

Scaling factor	9
Scaled vane chord (C)	59.4 cm
Axial chord/chord ( $C_{ax}/C$ )	0.48
Pitch/chord (P/C)	0.77
Span/chord (S/C)	0.93
Inlet Reynolds number ( $Re_{in}$ )	$2.2 \times 10^5$
Inlet mainstream velocity ( $U_{\infty, in}$ )	6.3 m/s
Inlet, exit flow angle	$0^\circ, 78^\circ$
Inlet, exit Mach number	0.017, 0.085

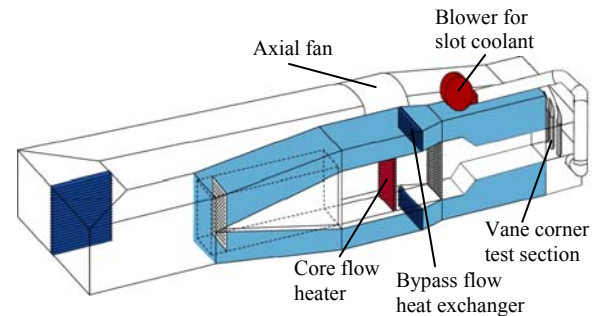


Figure 2. Depiction of the closed loop wind tunnel used in this study.

the bottom endwall, was described by a half-cosine that was a function of the distance along the vane surface. The fillet design parameters included the maximum fillet extent and height (cosine amplitude), the locations of the maximum extent and height relative to the vane stagnation (cosine phase), and the maximum distance of the fillet around the vane suction and pressure sides (cosine half-periods). This allowed the fillets to merge smoothly into the nominal manufacturing fillet (1.1 cm radius [0.019C]) while still maintaining the vane gage point. For this study, the linear fillet and the elliptical fillet had the same design parameters, and only differed in their endwall-to-airfoil profile.

The linear and elliptical fillets were machined from the same low-density foam as the vane. The fillets were positioned around the base of the vanes and sealed using silicone. Note that the baseline unfilleted endwall did not have a manufacturing fillet at the base of the vane, since the presence of the manufacturing fillet was shown by Lethander et al.<sup>5</sup> to not have an impact on the endwall flowfield.

**Table 2. Endwall and Fillet Geometry**

	Parameter	Value
Upstream slot	A – Location upstream of vane	0.37C (0.77C <sub>ax</sub> )
	B – Width	0.024C
	D – Flow length	1.88B
	E – Injection angle	45°
Leading edge fillet	F – Fillet LE to upstream slot	0.18C (0.38C <sub>ax</sub> )
	G – Maximum extent of fillet	0.16C
	H – Location of maximum extent/height around vane surface (from stagnation)	0.057C
	I – Maximum distance around PS	-0.87C
	J – Maximum distance around SS	0.57C
K – Maximum height of fillet	0.16C	

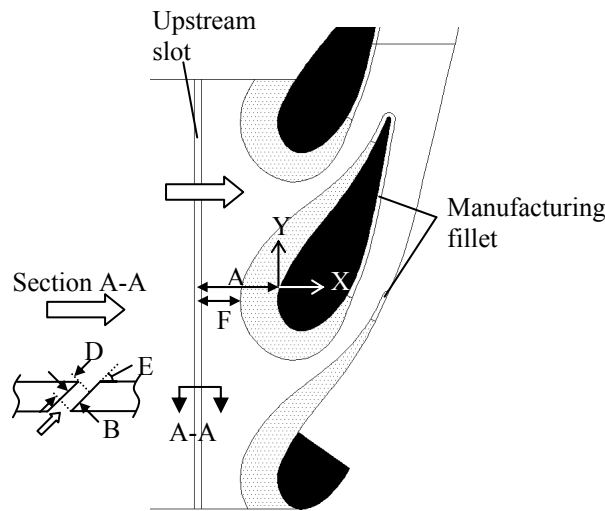


Figure 3. Schematic of the endwall and combustor-turbine interface gap (upstream slot).

### Aerodynamic Measurements

Measurements of streamwise velocity, yaw and pitch flow angles, and total pressure were obtained with a five-hole pressure probe at  $X/C_{ax}=1.02$ , slightly downstream of the vane trailing edge. The probe had a tip diameter of 2.41 mm (0.093”), and was nulled in yaw for each measurement point by rotating the probe until the difference in pressure between the side ports was nominally zero. Pressures from all five ports were sampled at 1000 Hz for 20 seconds and averaged to produce a single data point. Using calibration curves provided by the probe manufacturer (United Sensor), port pressures were used to determine total pressure, velocity magnitude, and pitch. Approximately 450 points were measured within the exit plane, which extended slightly more than one vane pitch (1.05P) across. To avoid probe interference effects, the closest measurement to the endwall was 6.35mm (1.2% span), and measurements were taken up to 203mm (37% span), where the flow was two-dimensional (no spanwise variation). Points were concentrated in regions of high gradients.

Uncertainties for the aerodynamic measurements were estimated by the partial derivative method. Yaw angle was estimated to be  $\partial\alpha=\pm 1.0^\circ$ . Pitch angle was estimated to be  $\partial\beta=\pm 0.14^\circ$ . Total pressure loss was estimated as  $\partial C_{P_{tot}}=\pm 0.017$  (6.1%) at a  $C_{P_{tot}}$  value of 0.28, and  $\partial C_{P_{tot}}=\pm 0.189$  (1.7%) at a  $C_{P_{tot}}$  value of 11.5.

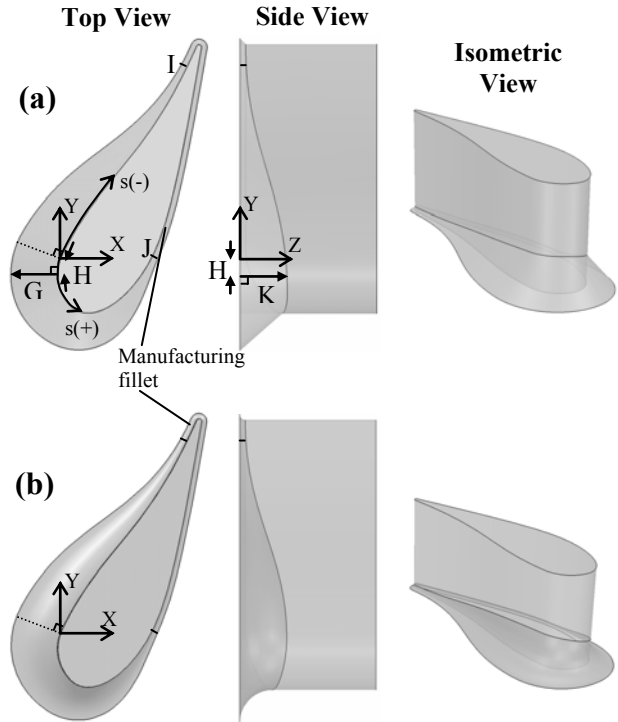


Figure 4. Geometrical parameters for an endwall-airfoil fillet with (a) a linear profile, and (b) an elliptical profile.

The largest contribution to uncertainty in  $C_{P_{tot}}$  was the uncertainty of the downstream total pressure measurement ( $\partial P_{tot} = \pm 0.4 \text{ Pa}$ ).

### Results

The measurements of pitchwise-averaged exit flow angles at the cascade exit plane for the three airfoil-endwall geometries are presented first, followed by total pressure losses. Contour plots of the total pressure loss in the exit plane, as well as averaged results, are presented. The results are interpreted by reviewing the previously reported experimental measurements of adiabatic cooling effectiveness from an upstream slot.

#### Exit Flow Angles

The pitchwise-averaged exit flow angle along the vane span is presented in Figure 5. Note that the figure shows exit flow angles relative to the midspan flow angle, to emphasize the effect of secondary flow. Exit flow angles that deviate from the design angle can lead to reduced aerodynamic performance of downstream airfoils. In Figure 5, for all airfoil-endwall geometries the endwall secondary flow causes overturning of the flow near the wall (sweeping of the flow toward the suction side of the adjacent vane), and underturning of the flow at approximately  $0.08S$ .

The effect of the various airfoil-endwall geometries is seen by comparing the solid lines in Figure 5. Both fillets appear to shift the point of minimum underturning toward midspan by about  $0.03S$ , when compared to the unfilleted airfoil case. Also, the overturning near the wall is reduced for both fillets as compared to the unfilleted airfoil. This trend of reduced near-wall turning would indicate a reduction in vortex

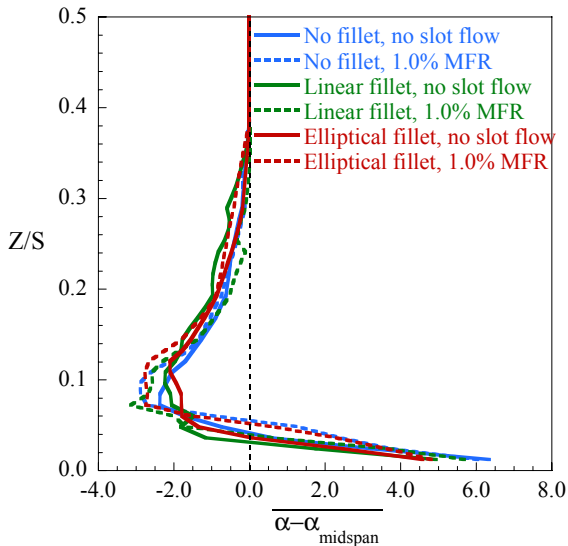


Figure 5. Pitchwise-averaged exit flow angle deviation from midspan for the three airfoil-endwall configurations.

strength, and is consistent with the findings of Becz et al.<sup>4</sup>, who noted that their fillet (similar to the elliptical fillet in this study) reduced near-wall turning for their blade geometry.

When leakage flow from the upstream slot at 1.0% MFR is added, the exit flow is further underturned compared to no flow at approximately  $0.08S$ , as seen by comparing the solid and dashed lines in Figure 5. This trend appears to be consistent among all of the airfoil-endwall geometries. However, below  $0.06S$  the addition of upstream leakage flow results in more turning toward the suction side for the unfilleted and elliptical fillet geometries than for the linear fillet geometry, or the cases without any slot flow. This possibly indicates a strengthening of the secondary flow features when leakage flow is added far upstream, as in this study.

#### Losses and Vorticity without Leakage Flow

Figure 6 presents contours of total pressure loss at the exit plane for the three airfoil-endwall configurations studied. Note that contours of axial vorticity are overlaid as black lines, with dashed black lines indicating negative vorticity. For the unfilleted case, the loss features are in agreement with measurements of secondary flow features. The large loss region from approximately  $Y/P = -0.04$  to  $0.12$  and extending to midspan is due to the airfoil wake. A mix of positive and negative vorticity islands in the wake near the endwall is due to the secondary flow vortices, as well as trailing filament vorticity caused by differential spanwise flow on the pressure and suction sides of the airfoil. A slight loss region and closed vorticity contour is centered around  $Y/P = 0.5$ , which is likely a weak vortex created by cross-passage flow. The elliptical loss region around  $Y/P = 0.8$  to  $0.9$  is due to the interaction of the passage and counter vortices. The closed vorticity contours with opposite signs delineate the two vortex structures at that location. The passage vortex, with positive vorticity, is located below the counter vortex. Finally, the increased losses and negative vorticity very close to the endwall, at both  $Y/P = 0.1$  to  $0.2$  and  $Y/P = 0.6$  to  $0.9$ , are indicative of the endwall boundary layer.

The linear fillet contours in Figure 6b show some notable differences from the baseline configuration in Figure 6a. The loss region indicating the interaction between the passage and counter vortices has been shifted toward midspan by about  $0.02S$  and reduced slightly. Also, the strength of the passage and counter vortices appears to be reduced. This is likely due to the effect of the fillet in reducing the horseshoe vortex strength and thus the strength of the passage and counter vortices. Finally, note that the loss due to the endwall boundary layer, as well as the vorticity in the boundary layer, have increased with the addition of the linear fillet. Previously reported results for endwall skin

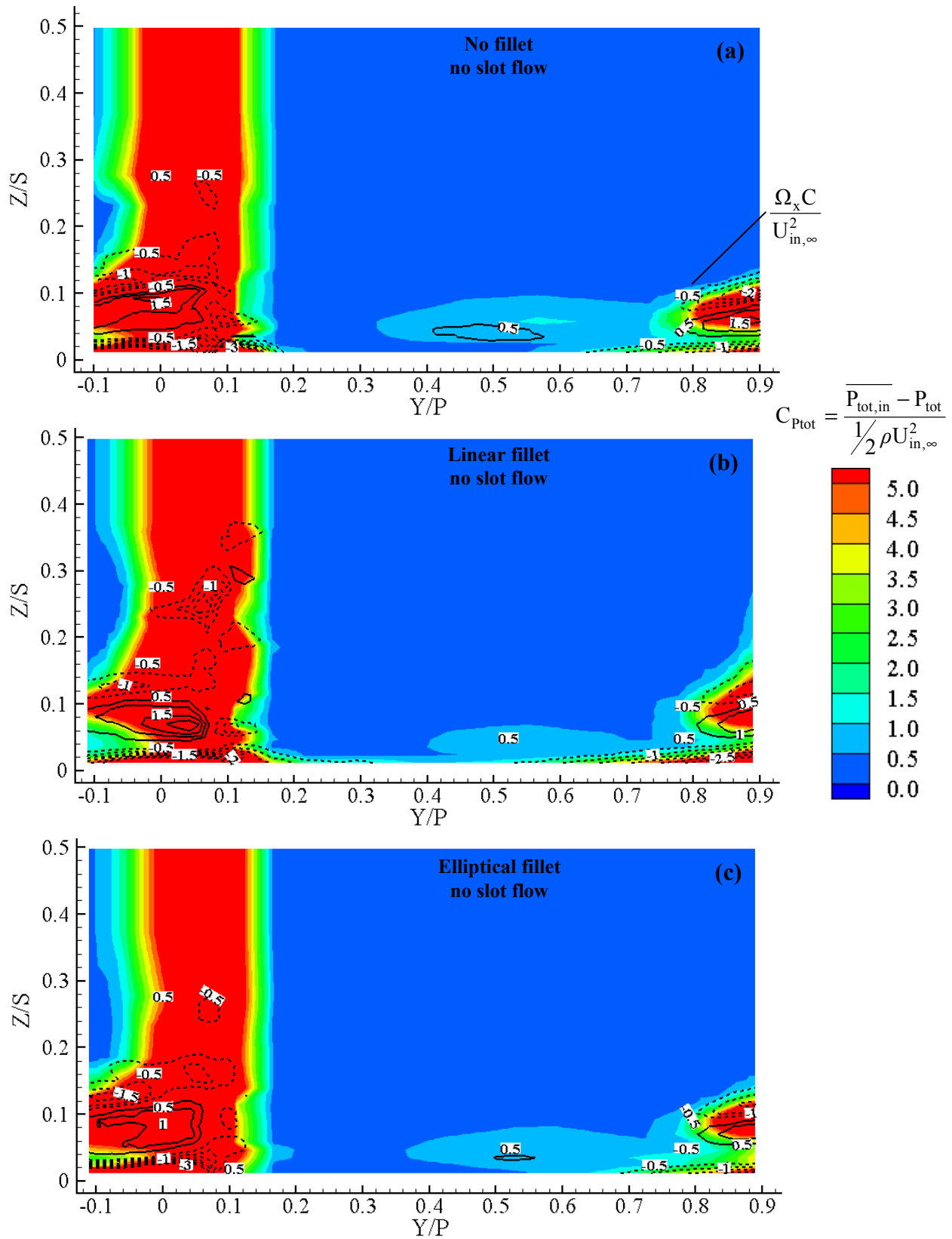


Figure 6. Contours of total pressure loss (color) overlaid with vorticity contours (black lines) at  $X/C_{ax}=1.02$ , for (a) no fillet, (b) a linear fillet, and (c) an elliptical fillet, all with no slot flow. Dashed lines indicate negative vorticity.

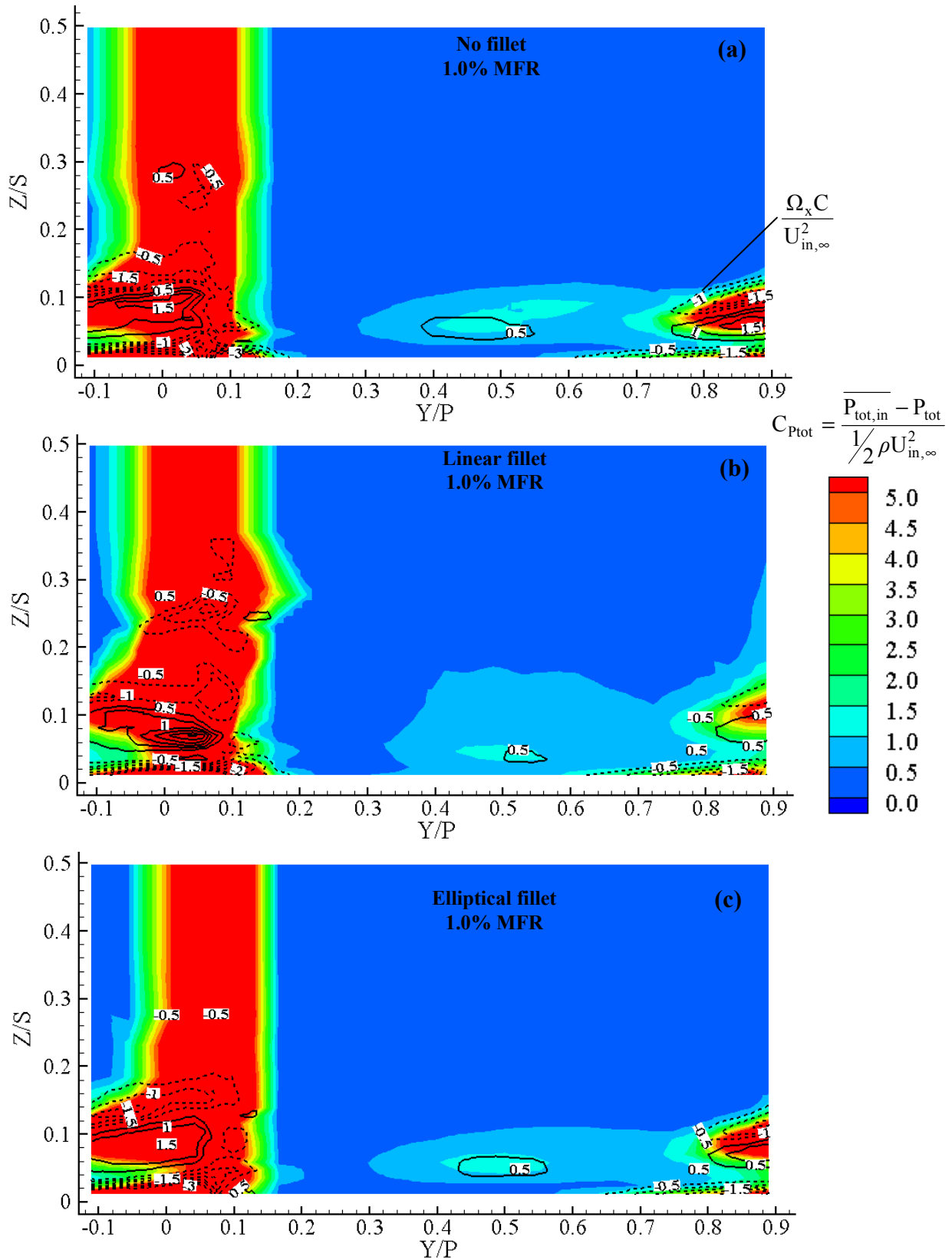


Figure 7. Contours of total pressure loss (color) overlaid with vorticity contours (black lines) at  $X/C_{ax}=1.02$ , for (a) no fillet, (b) a linear fillet, and (c) an elliptical fillet, all with 1.0% MFR. Dashed lines indicate negative vorticity.

friction also indicated increased shear with a linear fillet, although the overturning of the endwall streamlines was reduced as compared to the unfilleted case.

The elliptical fillet results in Figure 6c show a reduction in the size of the total pressure loss region, and reductions in the counter and passage vortex strengths, at  $Y/P=0.86$  when compared to the baseline case in Figure 6a. Again, this is consistent with the general effect of a fillet on the horseshoe vortex. Note, however, that the losses and vorticity near the endwall for the elliptical fillet are not as high as for the linear fillet, indicating that this type of fillet may have a more beneficial influence on the development of secondary flow features in the vane passage.

#### Losses and Vorticity with Leakage Flow

Contours of total pressure with vorticity overlaid are shown in Figure 7 for the three airfoil-endwall geometries with 1.0% MFR from the upstream slot. Note that for these cases with leakage flow, the upstream reference total pressure is the massflow-averaged total pressure of both the cascade inlet flow and the total pressure of the slot plenum, so that losses due to injection of the leakage flow through the slot are included in the total exit loss. Comparison of Figure 7a with Figure 6a shows the effect of leakage flow on the baseline unfilleted geometry. Most of the loss features are similar between the two cases. However, the loss region in the center of the passage (around  $Y/P=0.5$ ) is slightly increased with the addition of the leakage flow, and the loss region at the interaction of the passage and counter vortices at  $Y/P=0.86$  appears to be slightly larger. Figure 8 shows contours of the adiabatic film cooling effectiveness of the upstream leakage flow at 1.0% MFR, which were described in a previous report. In Figure 8a, it is apparent that most of the low-momentum upstream leakage flow is entrained in the horseshoe and passage vortex system, and thus contributes to the losses generated there. However, the low-momentum leakage flow may also have a secondary effect on the cross-passage flow and thus result in the increased loss seen in the center of the passage.

In comparing Figures 6b and 7b for the linear fillet, the effect of upstream slot leakage flow appears to have increased the extent of the loss region in the center of the passage. Interestingly, losses and vorticity have slightly decreased around  $Y/P=0.86$  for 1.0% MFR, which indicate that with a linear fillet, the addition of leakage flow further reduces the strength of the secondary flow vortices as compared to an unfilleted endwall. Figure 8b shows how the linear fillet tends to displace the leakage coolant around the base of the fillet and channel it into the passage vortex.

The elliptical fillet, shown without upstream slot flow in Figure 6c and with 1.0% MFR in Figure 7c, displays similar trends to the unfilleted endwall with and without slot flow. The loss region around  $Y/P=0.86$  is slightly larger, as well as the loss region in the center of the exit plane. However, the loss region and the vorticity in the center of the passage do not appear to have increased as much for the elliptical fillet when slot flow is added, as compared to the increase in the loss region for the unfilleted endwall when slot flow is added (compare Figures 6a and 7a). That is, the effect of the elliptical fillet on the endwall secondary vortices may be less sensitive to inlet flow perturbations such as upstream leakage flow.

#### Mass-Averaged Total Pressure Losses

Mass-averaged total pressure losses are presented in Figure 9 for all of the cases studied. Mass-averaged losses use the local mass flux to weight the total pressure loss in the averaging, and can be related to

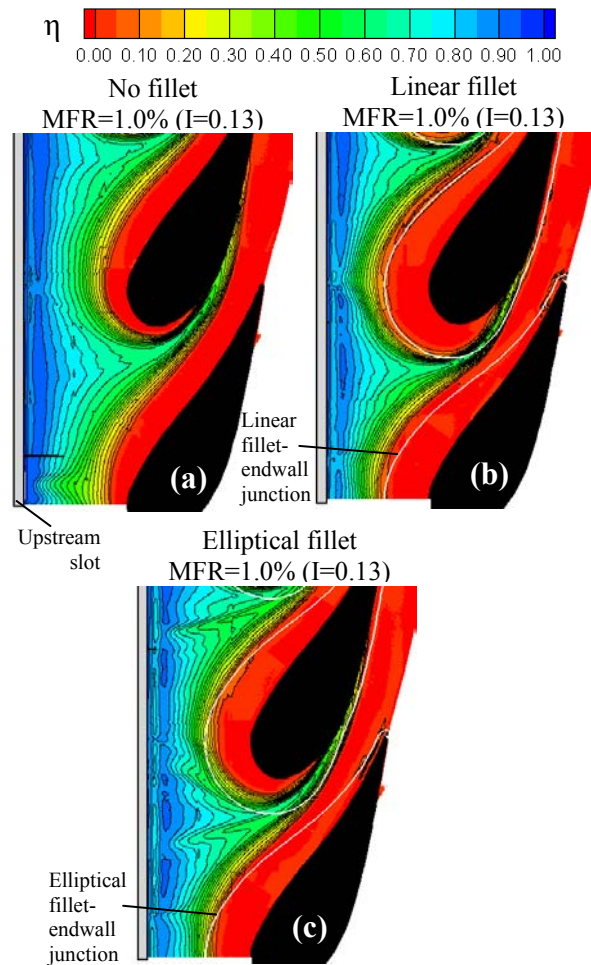


Figure 8. Adiabatic effectiveness contours for 1.0% upstream slot mass flow, with no fillet (a), a linear fillet (b), and an elliptical fillet (c).

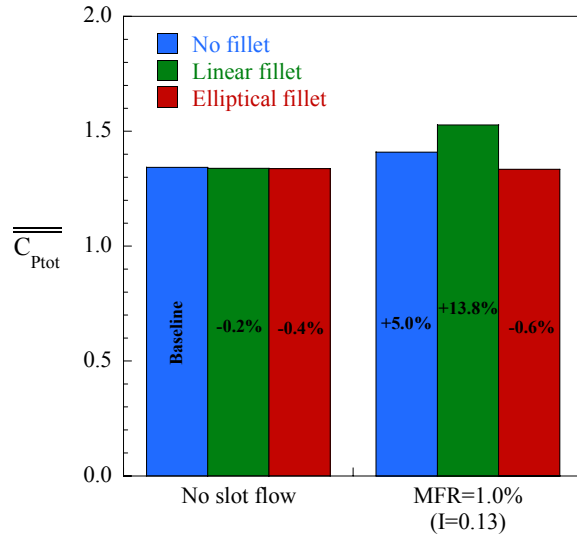


Figure 9. Mass-averaged total pressure loss for three airfoil-endwall geometries with and without leakage interface flow.

entropy generation (aerodynamic efficiency) in the cascade. The percentages indicated in the figure are increases or decreases relative to the baseline case of no fillet and no upstream leakage flow. In Figure 9, both the linear and elliptical fillet geometries result in a small decrease in mass-averaged total pressure loss as compared to the baseline. Lethander et al.<sup>5</sup> stated that their linear fillet geometry (same as for this study) resulted in a 1.6% increase in mass-averaged total pressure loss, as determined in their computational study, so large mass-averaged total pressure loss benefits were not expected with this fillet design.

The addition of upstream slot leakage flow resulted in an increase of mass-averaged total pressure loss for both the unfilleted and linear fillet cases. This agrees with the general trends seen the contours of Figures 6 and 7. The dramatic increase in loss for the linear fillet with 1.0% MFR from the upstream slot is likely due to the large loss region in the center of the exit plane in Figure 7b, as described earlier. As was seen in the loss contours of Figures 6c and 7c, the mass-averaged total pressure loss of the cascade with the elliptical fillet appears to be independent of the upstream leakage flow, which implies a reduced sensitivity to upstream conditions.

### Conclusions

Measurements of exit flow angle and total pressure loss were obtained for a vane cascade with and without two types of large fillets at the endwall-airfoil junction. Leakage flow was also introduced from a two-dimensional slot simulating the combustor-turbine interface gap.

Both the linear-profile fillet and the elliptical-profile fillet resulted in reduced overturning of the exit

flow angle near the wall, when no leakage flow was present. Addition of leakage flow caused larger values of overturning and overturning for all types of endwall-airfoil geometries, as compared to cases without leakage flow.

Loss regions and vorticity attributed to the passage and counter vortices were reduced for the linear fillet without leakage flow as compared to an unfilleted vane, although endwall losses were increased due to increased endwall shear. The elliptical fillet exhibited many of the same benefits as the linear fillet, but without increased endwall shear. Mass-averaging of the total pressure losses in the exit plane showed a slight decrease in loss for both fillet geometries as compared to the baseline.

The addition of leakage flow resulted in slightly increased losses for the vane with no fillet. Although the linear fillet showed a decrease in loss where the passage and counter vortices interacted, an increase in loss was seen in the remainder of the passage. The elliptical fillet did not appear to have increased loss with the addition of the leakage flow. Mass-averaged total pressure loss confirmed these trends, with increases in loss for the unfilleted and linear fillet geometries, and no change for the elliptical fillet geometry.

These results indicate that the use of a large fillet at the endwall-airfoil junction may reduce aerodynamic losses, but realistic inlet conditions should be taken into account to avoid unexpected interaction effects. Thus, turbine engine designers must carefully consider how a method of secondary flow control integrates with the complex inlet flowfield which results from gap interface leakage.

### Acknowledgments

The authors would like to thank the National Science Foundation's GOALI program and the Virginia Space Grant Consortium for funding this research. We would also like to acknowledge our partners in the GOALI program: Joel Wagner and Peter Tay (Pratt & Whitney), and Dr. Lee Langston and Brian Holley (University of Connecticut).

### Nomenclature

$C$	true chord of stator vane
$C_{ax}$	axial chord of stator vane
$C_{P_{tot}}$	total pressure loss, $C_{P_{tot}} = (\overline{P_{tot,in}} - P_{tot}) / \frac{1}{2} \rho U_{\infty,in}^2$
$\overline{\overline{C_{P_{tot}}}}$	Mass-averaged total pressure loss, $\overline{\overline{C_{P_{tot}}}} = \int C_{P_{tot}} \rho \vec{U} \cdot d\vec{A} / \int \rho \vec{U} \cdot d\vec{A}$
$H$	boundary layer shape factor

I	average momentum flux ratio, $I = \rho_c U_c^2 / \rho_\infty U_{\infty, \text{in}}^2$
LE	leading edge of airfoil
$\dot{m}$	mass flow rate
M	average blowing ratio, $M = \rho_c U_c / \rho_\infty U_{\infty, \text{in}}$
MFR	mass flow ratio, $MFR = \dot{m}_c / \dot{m}_{\text{in}}$
P	pitch of stator vane
$P_{\text{tot}}$	total pressure
$\overline{P_{\text{tot}, \text{in}}}$	massflow-averaged inlet total pressure, $\overline{P_{\text{tot}, \text{in}}} = (\dot{m}_{\text{in}} P_{\text{tot}, \text{in}} + \dot{m}_c P_{\text{tot}, \text{c}}) / (\dot{m}_{\text{in}} + \dot{m}_c)$
PS	pressure side of airfoil
$Re_{\text{in}}$	inlet Reynolds number, $Re_{\text{in}} = CU_{\infty, \text{in}} / \nu$
$Re_\theta$	momentum thickness Reynolds number, defined as $Re_\theta = \theta U_{\infty, \text{in}} / \nu$
S	span of stator vane
SS	suction side of airfoil
T	temperature
U	axial velocity
V	pitchwise velocity
W	spanwise velocity
X, Y, Z	vane coordinates, where X is turbine axial direction and Y is pitch direction

#### Greek

$\alpha$	yaw flow angle
$\beta$	pitch flow angle
$\delta$	boundary layer thickness
$\eta$	adiabatic effectiveness, $\eta = (T_\infty - T_{\text{aw}}) / (T_\infty - T_c)$
$\theta$	momentum thickness
$\nu$	kinematic viscosity
$\rho$	density
$\Omega_x$	axial vorticity, $\Omega_x = \partial V / \partial Z - \partial W / \partial Y$

#### Subscripts/Superscripts

aw	adiabatic wall
c	coolant conditions
in	inlet conditions
$\infty$	freestream conditions

#### References

- Langston, L.S., 1980, "Crossflows in a Turbine Passage," *Journal of Engineering for Power*, Vol. 102, pp. 866-874.
- Sauer, H., Muller, R., Vogeler, K., 2000, "Reduction of Secondary Flow Losses in Turbine Cascades by Leading Edge Modifications at the Endwall," ASME Paper 2000-GT-0473.
- Zess, G.A., Thole, K.A., 2002, "Computational Design and Experimental Evaluation of Using a Leading Edge Fillet on a Gas Turbine Vane," *ASME Journal of Turbomachinery*, Vol. 124, pp. 167-175.
- Becz, S., Majewski, M.S., Langston, L.S., 2004, "An Experimental Investigation of Contoured Leading Edges for Secondary Flow Loss Reduction," ASME Paper GT2004-53964.
- Lethander, A.T., Thole, K.A., Zess, G.A., Wagner, J., 2003, "Optimizing the Vane-Endwall Junction to Reduce Adiabatic Wall Temperatures in a Turbine Vane Passage," ASME Paper GT2003-38940.
- Han, S., Goldstein, R.J., 2005, "Influence of Blade Leading Edge Geometry on Turbine Endwall Heat (Mass) Transfer," ASME Paper GT2005-68590.
- Mahmood, G.I., Gustafson, R., Acharya, S., 2005, "Experimental Investigation of Flow Structure and Nusselt Number in a Low-Speed Linear Blade Passage With and Without Leading-Edge Fillets," *ASME Journal of Heat Transfer*, Vol. 127, pp. 499-512.
- Saha, A.K., Mahmood, G.I., Acharya, S., 2006, "The Role of Leading-Edge Contouring on End-wall Flow and Heat Transfer: Computations and Experiments," ASME Paper GT2006-91318.
- Blair, M.F., 1974, "An Experimental Study of Heat Transfer and Film Cooling on Large-Scale Turbine Endwalls," *Journal of Heat Transfer*, pp. 524-529.
- Knost, D. G., and Thole, K. A., 2005, "Adiabatic Effectiveness Measurements of Endwall Film-Cooling for a First Stage Vane," *Journal of Turbomachinery*, Vol. 127, pp. 297-305.
- Kost, F. and Nicklas, M., 2001, "Film-Cooled Turbine Endwall in a Transonic Flow Field: Part I- Aerodynamic Measurements," *Journal of Turbomachinery*, Vol. 123, pp. 709-719.
- Kost, F. and Mullaert, A., 2006, "Migration of Film-Coolant from Slot and Hole Ejection at a Turbine Vane Endwall," ASME Paper GT2006-90355.
- Burd, S.W., and Simon, T.W., 2000, "Effects of Slot Bleed Injection Over a Contoured Endwall On Nozzle Guide Vane Cooling Performance: Part I – Flow Field Measurements," ASME Paper 2000-GT-199.
- Burd, S.W., Satterness, C.J., and Simon, T.W., 2000, "Effects of Slot Bleed Injection Over a Contoured Endwall On Nozzle Guide Vane Cooling Performance: Part II - Thermal Measurements," ASME Paper 2000-GT-200.
- Cardwell, N.D., Sundaram, N., and Thole, K.A., 2007, "The Effects of Varying the Combustor-Turbine Gap," *Journal of Turbomachinery*, Vol. 123, pp. 756-764.
- Munson, B. R., Young, D. F., and Okiishi, T. H., 2002, *Fundamentals of Fluid Mechanics* (4th ed.), New York: John Wiley & Sons, Inc., p. 514.